A Longitudinal Model for Functional Connectivity Using Resting-State fMRI

Brian Hart[1], Ivor Cribben[2], Mark Fiecas[1], and for the Alzheimer's Disease Neuroimaging Initiative [*1]

[1]University of Minnesota
[2]University of Alberta

Abstract

Many neuroimaging studies collect functional magnetic resonance imaging (fMRI) data in a longitudinal manner. Repeated measures data calls for a longitudinal model which properly accounts for the natural correlation present in the data. In this work, we build a longitudinal functional connectivity model using a variance components approach. First, for all subjects' visits, we account for the autocorrelation inherent in the fMRI time series data using a non-parametric technique. Second, we use a generalized least squares approach to estimate the within-subject variance component shared across the population, the connectivity network, and the connectivity network's longitudinal trend. Our novel method seeks to account for the within-subject dependence across multiple visits, the variability due to the subjects being sampled from a population, and the autocorrelation present in fMRI data, while restricting the number of parameters in order to make the method computationally feasible and stable. We utilize a permutation testing procedure to draw valid inference on group differences in baseline connectivity and change in connectivity over time between a set of patients and a comparable set of controls. To examine performance, we run a series of simulations and apply the model to longitudinal fMRI data collected from the Alzheimer's Disease Neuroimaging Initiative database.

1 Introduction

Resting-state functional magnetic resonance imaging (fMRI) captures a series of images of the brain in subjects who are not given a particular task to perform while in the scanner. The scanner repeatedly captures blood oxygenation level dependent (BOLD) signals at hundreds of thousands of locations within the brain, creating a time series of images of the brain in a resting state. By capturing the BOLD signal of the resting brain, this imaging modality provides a chance for researchers to examine the intrinsic brain network of people from a certain population. The primary tool for doing so is the analysis of functional connectivity (FC) networks. We define FC as the temporal dependence in the blood oxygenation level dependent (BOLD) signals between brain regions [Fiecas et al., 2017]. Identifying group differences in FC can help better understand the underlying neurological process of a certain disease and its progression. Observed group differences can also potentially form biomarkers to be used for early detection and treatment of neurological disorders [Fox and Raichle, 2007].

Past research has identified altered FC between healthy aging patients and those that suffer from Alzheimer's disease (AD). Even among cognitively normal (CN) individuals, FC demonstrates aging effects that are heterogeneous between different brain regions [Chen et al., 2016]. Previous work also showed altered FC patterns beyond healthy aging in patients with dementia and AD [Chase, 2014, Hafkemeijer et al., 2012]. AD provides a perfect example of a condition that can be better understood through FC analysis. Many other works, including Ren et al. [2016] and Wang et al. [2007] have noted abnormal FC in various stages of AD. Wang et al. [2012] even demonstrated the impact of family history of AD on FC. In addition, Xiang et al. [2013] and Li et al. [2015] showed the link between decreased network connectivity and progression from a CN state, to mild cognitive impairment (MCI), and finally, to AD.

[*]Data used in preparation of this article were obtained from the Alzheimers Disease Neuroimaging Initiative (ADNI) database (adni.loni.usc.edu). As such, the investigators within the ADNI contributed to the design and implementation of ADNI and/or provided data but did not participate in analysis or writing of this report. A complete listing of ADNI investigators can be found at: `http://adni.loni.usc.edu/wp-content/uploads/how_to_apply/ADNI_Acknowledgement_List.pdf`

Altogether, these results suggest differing FC patterns between individuals with AD and their CN counterparts. Unfortunately, these analyses generally use ad hoc approaches that do not examine differences in both baseline connectivity and its longitudinal trend. Typically, massive univariate analyses are used in seed based models along with simple t-tests to test for group differences or longitudinal trend, or different connectivity metrics originally from graph theory are used to describe the networks. Many studies also do not account for the fact that, in practice, fMRI time series exhibit a moderate amount of autocorrelation [Worsley and Friston, 1995]. Failure to account for this autocorrelation may potentially lead to invalid inference. Additionally, of the previously mentioned studies, only Ren et al. [2016] utilizes truly longitudinal data. Aging effects are often measured by comparing a young group with an elderly group rather than following the same group of subjects over time. Finn and Constable [2016] demonstrated that CN patients have distinct brain signatures in fMRI images, implying that separate scans from a single individual exhibit some level of dependence. This finding can be leveraged in a longitudinal model which accounts for within-subject dependence to better model aging effects.

While longitudinal models exist for other neuroimaging modalities and metrics, no thorough general framework exists to draw inference on group differences in longitudinal fMRI FC. In this work, we propose a novel longitudinal model and inference procedure for FC in resting-state fMRI data. We seek to build a variance components FC model which accounts for the within-subject dependence across multiple visits, the variability due to the subjects being sampled from a population, and any autocorrelation present in fMRI time series. We also propose a inference procedure that allows for valid hypothesis testing of group differences in baseline connectivity networks and connectivity network aging effects.

2 Materials and Methods

2.1 Model Specification

Suppose we have a cohort of N individuals from two different groups, such that there are N_1 and N_2 participants in groups 1 and 2, respectively. We collect a P-variate, detrended time series of length T from the preprocessed fMRI images of each the N subjects at each visit. To keep the dimensionality of the data reasonable in a whole network analysis, we condense the data to the region of interest (ROI) level with a time series for each ROI at each visit. Here we define the ROI level time series as the average of the time series from each voxel within a region of the brain. Let the subscripts i and j denote subject and visit respectively. A particular subject returns for J_i total visits. Let Y_i represent the vector of sample correlation coefficients of length QJ_i, where $Q = P(P-1)/2$ is the number of ROI pairs. Within Y_i, the Q correlations from the first visit are followed by the Q correlations from the second visit and so on until the J_ith visit. The model is fit separately to each group. The baseline effect specific to group G, β_{0G}, repeats the length Q baseline effect J_i times. The covariate v_i represents a vector which repeats the visit times for subject i, Q times each. Depending on the nature of the data and the research questions at hand, v_{ij} can be set to the visit number, the time since baseline, or the patient's age. We use β_{1G} to denote the group specific longitudinal trend. We split the variance term ε_i into two components: a block diagonal term, Σ_i, containing $Q \times Q$ matrices Σ_{ij} along the diagonal which represent the within visit covariance unique to each visit, and a within-subject term, Ψ_G, shared by all subjects in group G. Our model has the following linear form:

$$Y_i = \beta_{0G} + v_i\beta_{1G} + \varepsilon_i, \quad \text{where} \quad \text{Var}(\varepsilon_i) = \Sigma_i + \Psi_G. \tag{1}$$

The shared within-subject covariance Ψ_G can be additionally broken down into two components: Ψ_{0G} and Ψ_{1G}. Ψ_{0G} is a block diagonal structure with a $Q \times Q$ block repeated along the diagonal and models the within-visit covariability not captured by Σ. This term captures the variance that arises from sampling from the general population. Then Ψ_{1G} fills the remaining off diagonal $Q \times Q$ blocks of Ψ_G and models the within-subject, across visit covariability. This term captures the dependence between multiple visits from the same subject. The model can equivalently be written in the matrix form as $Y_i = X_i\beta_G + \varepsilon_i$. Using this notation, we show clearly the structure of our model in Figure 1. Figure 2 shows a workflow chart of the procedure used to estimate the model parameters and test hypotheses which are subsequently described in more detail.

2.2 Estimating Within Visit Covariance

We start by estimating the sample correlation coefficient between all ROI pairs for all visits. Let $(w_{1t}, ..., w_{pt})'$ for $t \in (1, 2, ..., T)$ be the P-variate time series from a single visit. Then for two ROIs, a and b, with $a \neq b$, we have

$$r_{ab} = \frac{\sum_{t=1}^{T}(w_{at} - \bar{w}_a)(w_{bt} - \bar{w}_b)}{\sqrt{\sum_{t=1}^{T}(w_{at} - \bar{w}_a)^2 \sum_{t=1}^{T}(w_{bt} - \bar{w}_b)^2}}. \tag{2}$$

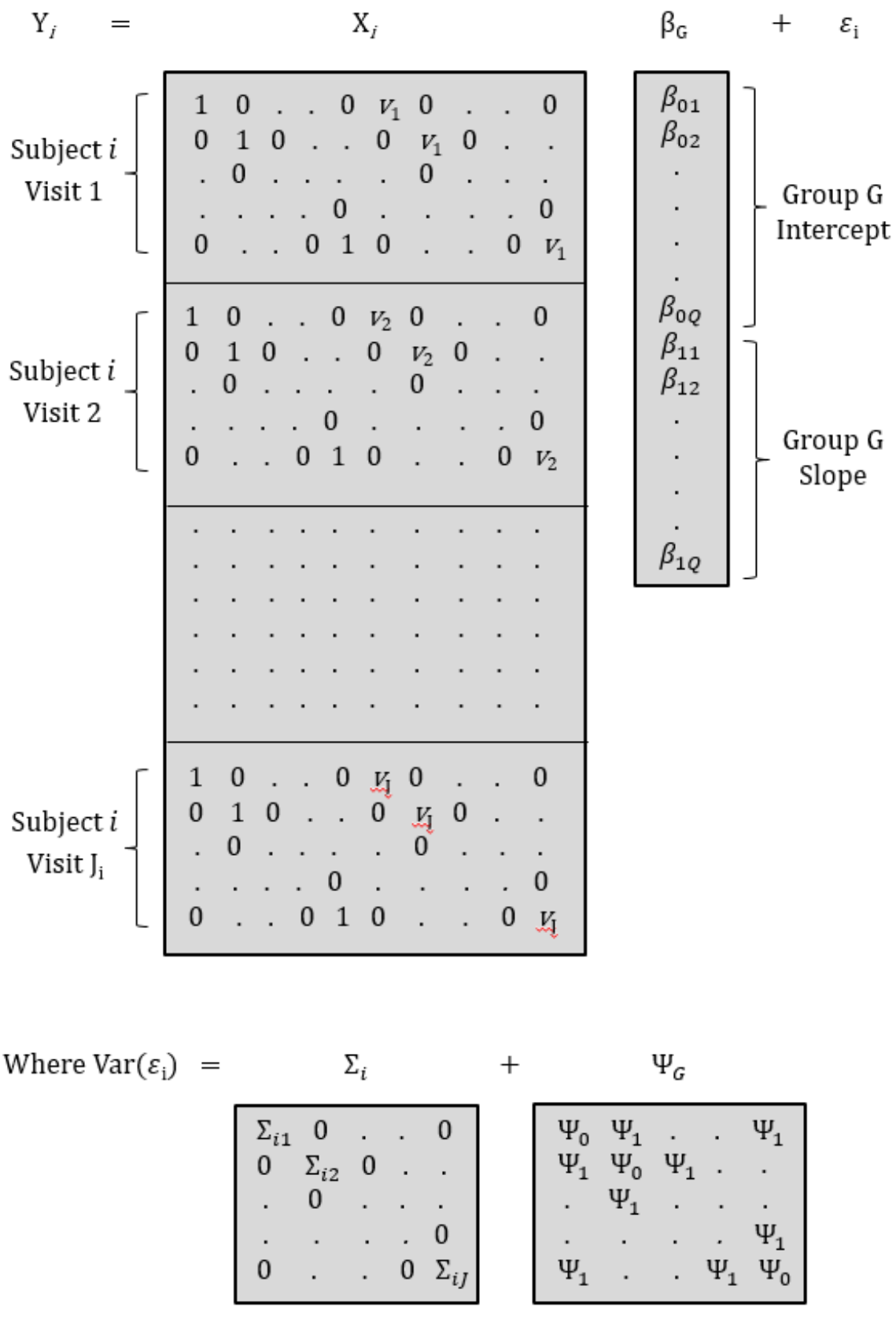

Figure 1: The structure of our variance components model for a given subject.

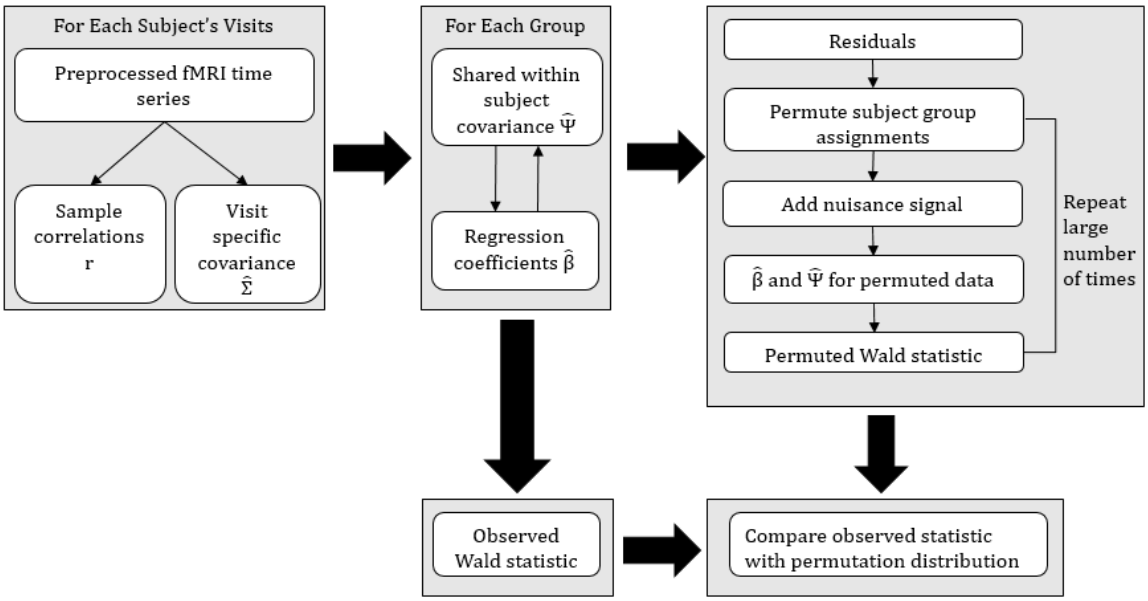

Figure 2: A workflow chart of the estimation and inferential procedure of our variance components model.

Frequently, a Fisher transform, $g(x) = tanh^{-1}(x) = 0.5\log(1+x)/(1-x)$, is applied to the resulting correlations as a variance stabilizing transformation so that $\sqrt{T}(g(r_{ab}) - g(\rho_{ab})) \xrightarrow{D} N(0,1)$. Unfortunately, this approach assumes the observations from the time series are independent and therefore leads to invalid inference due to the inherent autocorrelation in fMRI time series data. To account for autocorrelation we use a result of Roy [1989]. Let a, b, c, and d be ROIs where $a \neq b$ and $c \neq d$. We then define r_{ab} as in Equation (2) and likewise for r_{cd}. Then, under mild conditions, Roy [1989] derived the following large-sample covariance of r_{ab} and r_{cd}:

$$\begin{aligned} Cov(r_{ab}, r_{cd}) \approx [&0.5\rho_{ab}\rho_{cd}(\Delta(a,c,a,c) + \Delta(a,d,a,d) + \Delta(b,c,b,c) + \Delta(b,d,b,d)) \\ &- \rho_{ab}(\Delta(a,c,a,d) + \Delta(b,c,b,d)) - \rho_{cd}(\Delta(b,c,a,c) + \Delta(b,d,a,d)) \\ &+ \Delta(a,c,b,d) + \Delta(b,c,a,d)]/T. \end{aligned} \tag{3}$$

Here we define $\rho_{ab}(u) = Corr(w_{at}, w_{b,t+u})$ and $\Delta(a,b,c,d) = \sum_{u=-\infty}^{\infty} \rho_{ab}(u)\rho_{cd}(u)$. Equivalently, using cross-covariance instead of cross-correlation, we define

$$\Delta(a,b,c,d) = \frac{\Theta(a,b,c,d)}{\sqrt{(\gamma_{aa}(0)\gamma_{bb}(0)\gamma_{cc}(0)\gamma_{dd}(0))}}, \tag{4}$$

where $\Theta(a,b,c,d) = \sum_{u=-\infty}^{\infty} \gamma_{ab}(u)\gamma_{cd}(u)$ and $\gamma_{ab}(u) = Cov(w_{at}, w_{b,t+u})$.

To estimate $Cov(r_{ab}, r_{cd})$ for each combination of ROI pairs (a,b) and (c,d), we start by estimating $\gamma_{ab}(u)$ as

$$\hat{\gamma}_{ab} = \frac{\sum_{t=1}^{T-u} w_{at}w_{b,t+u}}{T}. \tag{5}$$

Next, we use the estimates of γ_{ab} to obtain

$$\hat{\Theta}(a,b,c,d) = \sum_{u=-T+1}^{T-1} h_u^2 \hat{\gamma}_{ab}(u)\hat{\gamma}_{ld}(u), \tag{6}$$

where $h(\cdot)$ is some taper function with bandwidth $b = b(T)$. Any reasonable taper choice leads to very similar estimates, so we proceed with the modified Bartlett window [Melard et al., 1991, Fiecas et al., 2017]. We now have a consistent estimator of $\Delta(a,b,c,d)$ by plugging the results of equations (5) and (6) into equation (4). Finally, using equation (3), plugging in r_{ab} for ρ_{ab} and $\hat{\Delta}(a,b,c,d)$ for $\Delta(a,b,c,d)$, we can estimate $Cov(r_{ab}, r_{cd})$ for each combination of ROI pairs (a,b) and (c,d).

2.3 Estimating Between Subject Covariance, Ψ, and β

We now proceed with the estimation of the between subject covariance Ψ and the regression coefficients β, conditional on the previously estimated within-visit covariances, $\hat{\Sigma}_{ij}$. We use the same procedure to estimate each group's parameters separately, so in the formulas in the following description of the single group estimation procedure we drop the subscript G. Utilizing a generalized least squares (GLS) approach, we update $\hat{\Psi}$ and $\hat{\beta}$.

Although the framework allows for many different structures for Ψ, we assume a block compound symmetry structure so that all diagonal blocks, Ψ_0, are equal and all off diagonal blocks, Ψ_1, are equal. The block compound symmetry assumption keeps the parameter space to a reasonable size. To initiate the estimation process we use the ordinary least squares estimator $\hat{\beta} = (X'X)^{-1}X'Y$ to provide a good starting estimate of β. We then update the two components of Ψ using the following formulas:

$$\hat{\Psi}_0 = \frac{1}{\sum_{i=1}^{N} J_i} \sum_{i=1}^{N} \sum_{j=1}^{J_i} (Y_{ij} - X_{ij}\hat{\beta})'(Y_{ij} - X_{ij}\hat{\beta}) - \hat{\Sigma}_{ij}, \quad \text{and} \tag{7}$$

$$\hat{\Psi}_1 = \frac{1}{\sum_{i=1}^{N} \frac{J_i(J_i-1)}{2}} \sum_{i=1}^{N} \sum_{j \neq k} (Y_{ij} - X_{ij}\hat{\beta})'(Y_{ik} - X_{ik}\hat{\beta}). \tag{8}$$

These estimators bear a resemblance to the mean squared error. For $\hat{\Psi}_0$, the sum of the squared residuals for all visits are summed. Then to obtain the final estimate, we subtract the previously estimated variance component $\hat{\Sigma}$ and divide the covariance matrix by the total number of visits. We estimate Ψ_1 in a similar fashion. In this case, we calculate and average the cross products of the residuals from all pairs of visits for each subject. We do not subtract the $\hat{\Sigma}$ term here because $\hat{\Sigma}$ has been set to 0 for the off diagonal blocks occupied by Ψ_1. These simple estimators, obtained through matching moments, provide a significant reduction in computation in comparison with a maximum likelihood approach.

With an estimate of Ψ, we can now use the standard GLS formula to update the regression coefficients as follows: $\hat{\beta} = (X'(\hat{\Sigma} + \hat{\Psi})^{-1}X)^{-1}X'(\hat{\Sigma} + \hat{\Psi})^{-1}Y$. At this point we have two choices: to iteratively update $\hat{\Psi}$ and $\hat{\beta}$ until convergence (full convergence), or accept the estimates (one-step) and proceed with the inferential procedure. The one-step estimator provides a significant advantage in computing time as $\hat{\Psi}$ and $\hat{\beta}$ must be estimated for each permutation of the inference procedure [Ganjgahi et al., 2015]. Additionally, Amemiya [1977] proved that the one-step GLS estimator maintains consistency. In both the full convergence and one-step versions of the model, estimates are calculated for each group separately before proceeding with hypothesis testing.

2.4 Inference

Two general hypothesis tests are of interest in a longitudinal FC model: the group difference between the baseline connectivity, and the group difference in the rate of change in connectivity. For each hypothesis, we would also like to test for the significance of the group differences in both the global connectivity networks and the local ROI pair connectivity. To accomplish these objectives, we use the Wald statistic, $(C(\hat{\beta}_{G1} - \hat{\beta}_{G2}))'[C(\widehat{\text{Var}}(\hat{\beta}_{G1}) + \widehat{\text{Var}}(\hat{\beta}_{G2}))C']^{-1}C(\hat{\beta}_{G1} - \hat{\beta}_{G2})$, and adjust the contrast matrix, C, depending on the hypothesis of interest.

We estimate the variance of each group's regression coefficients using $\widehat{\text{Var}}(\hat{\beta}_G) = (X_G'(\hat{\Sigma}_G + \hat{\Psi}_G)^{-1}X_G)^{-1}$. While the Wald statistic is asymptotically χ^2 with degrees of freedom equal to the rank of C, the asymptotic distribution poorly approximates the finite sample distribution with a moderate number of ROIs. Instead of relying on asymptotics, we propose a permutation procedure for all inference. Chung et al. [2013] shows that using a studentized test statistic, such as the proposed Wald statistic, allows for valid inference in many permutation test settings. Omelka and Pauly [2012] confirmed these results for our current setting of two sample tests of correlation coefficients.

We use a permutation strategy suggested by Ganjgahi et al. [2015] and originally proposed by Ter Braak [1992]. A recent comparison of the performance of many different permutation strategies by Winkler et al. [2014] shows that the Ter Braak permutation testing procedure maintains nominal Type I error and is fairly robust. This method offers the additional advantage that the data only needs to be permuted once and the model only fit twice at each iteration of the permutation test in order to test all local and global hypotheses. Testing all hypotheses under a single permutation schedule greatly reduces the computational burden of the testing procedure.

The permutation testing procedure is performed as follows:

1. Calculate residuals from the fitted model for each subject: $e_i = Y_i - \hat{\beta}_{0G} - v_i\hat{\beta}_{1G}$ with subject i in group G.
2. Permute group assignments of e_i.
3. Add the nuisance signal back to e_i based on new permuted group assignments G^*. For the main effect (intercept) tests we add in the longitudinal trends by setting $e^*_{ij} = e_{ij} + v_{ij}\hat{\beta}_{1G^*}$. Likewise, for the interaction (slope) tests we set $e^*_{ij} = e_{ij} + \hat{\beta}_{0G^*}$.

4. Refit the model on e^*.
5. Calculate a new Wald statistic for the fitted values of $\hat{\beta}^*$ and $\hat{\Psi}^*$.

We repeat this process a large number of times to create a permutation distribution to be used as a reference distribution of the originally calculated test statistic. Because the obtained p-values are estimated, we additionally use the permutation p-value correction procedure of Phipson et al. [2010]. To account for the fact that $2Q$ local hypotheses are tested simultaneously, we then apply the false discovery rate (FDR) controlling procedure of Benjamini and Hochberg [1995] to the corrected p-values from the local tests. The Phipson correction helps avoid unadjusted p-values with value 0 which may improperly maintain significance after a multiple comparisons correction.

2.5 Simulated Data

A series of simulations were designed with different data generating mechanisms to assess model performance. In all scenarios each time series contained 120 time points with autocorrelation that followed a first-order autoregressive process with an AR parameter of 0.3. A multivariate time series was simulated for each subject at three visits. For each visit, the Q correlations were simulated from a multivariate normal distribution where the mean and variance varied by group based on the simulation setting. For group 1, the mean vector was always assumed to be 0 and the covariance matrix was the same across all simulation settings. The simulations used either 3, 5, or 10 as the dimension of the multivariate normal distribution. For the 3 and 5 dimension settings only the first element of the group 2 mean vector was allowed to vary by simulation setting, while the other elements were set to match group 1. For the 10 dimension settings the first 5 elements of the group 2 mean vector varied by simulation setting. 1,000 Monte Carlo simulations were run for all simulation settings with 3 and 5 dimensions, and 500 simulations were run for the 10 dimensional simulation settings. Group sizes of 15 and 30 were considered. The true variance of the correlations was either equal for the two groups or the group 2 variance was double the group 1 variance. 500 permutations were used for the permutation test for all settings.

To increase model parsimony, different structures can be considered for Σ_{ij}, Ψ_0, and Ψ_1. In the simulation study, we use scaled identity or compound symmetry structures for the two Ψ components. We estimate these components by setting all diagonal elements of each matrix to the average of the diagonal elements and likewise for the off diagonal elements [Laird, 2004]. For Σ_{ij} we consider unstructured and diagonal options.

Three models were fit to each simulated dataset. The first was a full convergence model which iterated between $\hat{\Psi}$ and $\hat{\beta}$ until convergence. It assumed an unstructured Σ_{ij} and compound symmetry for Ψ_0 and Ψ_1. This model is referred to as the full convergence full variance model. The second was a one-step model which stops after one iteration of solving for $\hat{\Psi}$ and $\hat{\beta}$. It also assumed an unstructured Σ_{ij} and compound symmetry for Ψ_0 and Ψ_1, and it is referred to as the one-step convergence full variance model. The final model was a one-step model which assumed a diagonal structure for Σ_{ij} and scaled identity structures for Ψ_0 and Ψ_1. The last model is referred to as the one-step convergence reduced variance model.

2.6 ADNI Data

Data used in the preparation of this article were obtained from the Alzheimers Disease Neuroimaging Initiative (ADNI) database (`http://adni.loni.usc.edu`). The ADNI was launched in 2003 as a public-private partnership, led by Principal Investigator Michael W. Weiner, MD. The primary goal of ADNI has been to test whether serial magnetic resonance imaging (MRI), positron emission tomography (PET), other biological markers, and clinical and neuropsychological assessment can be combined to measure the progression of MCI and early AD. For up-to-date information, see `www.adni-info.org`.

A subset of the ADNI data was used to demonstrate a practical application of the model. The data consists of longitudinal resting-state fMRI images collected at baseline, 3 months from baseline, 6 months from baseline, 12 months from baseline, and annually thereafter. There are two disease groups of interest, the CN group and the AD group. We focused our attention on late-onset AD and included only patients that were 65 years of age or older at baseline [van der Flier et al., 2011, Holland et al., 2012]. To better separate the AD and CN groups, only patients that remained in one group for the entirety of the follow-up were considered in our analysis. The remaining CN group consists of 111 visits from 30 patients (17 females and 13 males) with each patient having between 1 and 6 visits. The AD group consists of 79 visits from 26 patients (11 females and 15 males) with each patient having between 1 and 5 visits. The average age was 75.9 for the CN group with a range of 65.2 to 95.7. The AD group average age was 76.7 with a range of 66.5 to 88.6.

2.6.1 Preprocessing

We preprocessed the data using both FSL (version 5.0.9, `https://fsl.fmrib.ox.ac.uk/`) and AFNI (version AFNI_17.0.15, `https://afni.nimh.nih.gov/`). The preprocessing steps were as follows. We 1) applied motion

correction to the images using FSL's mcflirt (rigid body transform; cost function normalized correlation; reference volume the middle volume) and then 2) normalized the images into the Montreal Neurological Institute space using FSL's flirt (affine transform; cost function correlation ratio). We used FSL's fast to 3) obtain a probabilistic segmentation of the brain to obtain white matter and cerebrospinal fluid (CSF) probabilistic maps, thresholded at 0.75. Using FSL's fslmaths, we 4) spatially smoothed the volumes using a Gaussian kernel with FWHM=5 mm. We used AFNI's 3dDetrend to 5) remove nuisance signals, namely the six motion parameters, white matter and CSF signals, and the global signal. Finally, 6) the linear trend was removed from each time series using linear regression and a 4th order Butterworth low-pass filter with a 0.1 Hertz cutoff was applied to each fMRI time series.

2.6.2 Analysis

Ten ROIs from the ADNI dataset were selected for analysis: left and right hippocampus (HC), parahippocampus (PHC), posterior cingulate (PCC), precuneus (PQ), and prefrontal cortex (PFC). In all results that follow an l suffix for an ROI denotes the left side of the brain and an r suffix denotes the right side. We selected these ROIs because they make up the hippocampi and the default mode network (DMN) in which FC has been shown to differ between CN and AD groups [Supekar et al., 2008, Greicius et al., 2004, Sorg et al., 2007].

Four versions of the model were fit to the ADNI data with differing assumptions. The first (Model 1) is a one-step estimation model which assumes a compound symmetry structure for Ψ_0 and Ψ_1 and unstructured diagonal blocks for Σ. The next (Model 2), makes the same assumptions for Ψ_0, Ψ_1, and Σ but uses the full convergence estimator. Model 3 is a one-step estimation model assuming scaled identity structures for Ψ_0 and Ψ_1 and a diagonal structure for Σ. The final model (Model 4) is a one-step estimation model which assumes a diagonal structure for Ψ_0, sets all elements of Ψ_1 to 0, and assumes a diagonal structure for Σ. This final model is equivalent to a massive univariate approach which ignores the within-subject dependence. 5,000 permutations were run for the permutation test for all models. The intercept of each model represents the FC network of each group at age 65.

3 Results

3.1 Simulated Data

Tables 1 and 2 show results from the simulation study. Table 1 shows the global and local Type I error for the main effect and interaction across all simulations. The reported global test results are the average global Type I errors across 500 or 1,000 Monte Carlo runs. The local test results are the average Type I errors of the unadjusted p-values for all null hypotheses across the 500 or 1,000 Monte Carlo runs. While the local p-values would be adjusted in practice, the numbers in the table provide easy reference to a nominal Type I error of 0.05. Table 2 shows the average global power and average local power using false discovery rate adjusted p-values. All p-values were corrected using the method of Phipson et al. [2010].

3.2 ADNI Data

Table 3 shows results from the global hypothesis tests and all local hypothesis tests that were significant before p-value adjustment for Model 1. The results for the other three models can be found in Table S2 from Supplement A. Neither the overall main effect or interaction term were found to be significantly different in the global tests for any of the four models considered. The only ROI pair level difference that remained significant after p-value adjustment and correction in any of the models was the difference in the CN and AD group slopes in the connectivity between the left HC and the right PCC in Models 1 and 2. These models conclude that the connectivity between the left HC and the right PCC declines at a much quicker rate in the AD population than in their CN counterparts. The estimated group intercepts, group longitudinal trends, group differences in intercepts and longitudinal trends, and $-\log_{10}$ p-values after correction and adjustment from local hypothesis tests are presented graphically in Figure 3 for Model 1 and Figures S1, S2, and S3 from Supplement A for Models 2, 3, and 4, respectively.

4 Discussion

4.1 Simulated Data

The Type I error results from Table 1 show roughly nominal Type I error rates for all three models fit to the simulated data. While there is some slight inflation in all three models, especially for the 10 ROI simulations, the

Table 1: Type I error rates for simulation study. for all globally null simulation settings. Type I errors for the main effect (group difference in intercepts) and interaction effect (group difference in slopes) are reported both globally and locally. The global Type I errors are averaged across all models. The local Type I errors reported are unadjusted and averaged across all simulations and all null ROI pairs.

		Convergence Type:			**Full**		**One-Step**			**One-Step**	
		Variance Structure:			**Full**		**Full**			**Reduced**	
	Group Size	**Variance**	β_0	β_1	**3 ROIs**	**5 ROIs**	**3 ROIs**	**5 ROIs**	**10 ROIs**	**3 ROIs**	**5 ROIs**
Main Effect Global Test	**15**	**Equal**	**0**	**0**	0.061	0.052	0.057	0.055	0.066	0.056	0.054
			0	**0.1**	0.065	0.065	0.067	0.071	0.064	0.067	0.063
		Group 2	**0**	**0**	0.058	0.049	0.055	0.053	0.054	0.056	0.048
		Double	**0**	**0.1**	0.068	0.058	0.069	0.056	0.068	0.070	0.060
	30	**Equal**	**0**	**0**	0.045	0.049	0.046	0.050	0.066	0.043	0.047
			0	**0.1**	0.046	0.050	0.054	0.047	0.066	0.048	0.049
		Group 2	**0**	**0**	0.057	0.054	0.058	0.053	0.062	0.058	0.060
		Double	**0**	**0.1**	0.049	0.066	0.055	0.059	0.078	0.058	0.053
Main Effect Local Test	**15**	**Equal**	**0**	**0**	0.071	0.061	0.073	0.061	0.066	0.066	0.062
			0	**0.1**	0.064	0.067	0.067	0.069	0.069	0.064	0.067
		Group 2	**0**	**0**	0.064	0.063	0.061	0.062	0.071	0.064	0.064
		Double	**0**	**0.1**	0.068	0.062	0.069	0.063	0.069	0.065	0.063
	30	**Equal**	**0**	**0**	0.050	0.059	0.048	0.058	0.058	0.048	0.057
			0	**0.1**	0.053	0.058	0.051	0.058	0.056	0.052	0.057
		Group 2	**0**	**0**	0.063	0.055	0.062	0.055	0.057	0.060	0.056
		Double	**0**	**0.1**	0.054	0.059	0.055	0.058	0.059	0.053	0.057
Interaction Global Test	**15**	**Equal**	**0**	**0**	0.062	0.054	0.052	0.057	0.072	0.049	0.052
			0.1	**0**	0.046	0.054	0.044	0.049	0.076	0.044	0.049
		Group 2	**0**	**0**	0.057	0.067	0.050	0.062	0.070	0.051	0.069
		Double	**0.1**	**0**	0.079	0.071	0.078	0.061	0.090	0.073	0.063
	30	**Equal**	**0**	**0**	0.054	0.059	0.058	0.061	0.078	0.056	0.058
			0.1	**0**	0.052	0.067	0.049	0.063	0.070	0.051	0.051
		Group 2	**0**	**0**	0.068	0.065	0.071	0.061	0.072	0.075	0.057
		Double	**0.1**	**0**	0.056	0.041	0.057	0.049	0.068	0.059	0.040
Interaction Local Test	**15**	**Equal**	**0**	**0**	0.059	0.062	0.058	0.062	0.067	0.059	0.064
			0.1	**0**	0.055	0.060	0.054	0.057	0.071	0.057	0.060
		Group 2	**0**	**0**	0.063	0.065	0.065	0.061	0.072	0.064	0.063
		Double	**0.1**	**0**	0.074	0.067	0.071	0.061	0.067	0.074	0.064
	30	**Equal**	**0**	**0**	0.050	0.055	0.049	0.054	0.059	0.049	0.055
			0.1	**0**	0.054	0.059	0.053	0.058	0.056	0.058	0.059
		Group 2	**0**	**0**	0.061	0.059	0.062	0.057	0.060	0.063	0.060
		Double	**0.1**	**0**	0.057	0.055	0.057	0.055	0.058	0.058	0.055

Table 2: The power calculations for the simulation study. Power results for the main effect (group difference in intercepts) and interaction effect (group difference in slopes) are reported both globally and locally. The global power results are averaged across all models. The local power results reported are unadjusted and averaged across all simulations and all non-null ROI pairs.

		Convergence Type:			**Full**		**One-Step**			**One-Step**	
		Variance Structure:			**Full**		**Full**			**Reduced**	
	Group Size	**Variance**	β_0	β_1	**3 ROIs**	**5 ROIs**	**3 ROIs**	**5 ROIs**	**10 ROIs**	**3 ROIs**	**5 ROIs**
Main Effect Global Test	**15**	**Equal**	**0.1**	**0**	0.382	0.223	0.369	0.229	0.482	0.372	0.211
			0.1	**0.1**	0.389	0.214	0.390	0.203	0.466	0.391	0.204
		Group 2	**0.1**	**0**	0.300	0.196	0.294	0.185	0.356	0.303	0.185
		Double	**0.1**	**0.1**	0.328	0.180	0.321	0.170	0.386	0.316	0.177
	30	**Equal**	**0.1**	**0**	0.674	0.491	0.679	0.489	0.902	0.682	0.469
			0.1	**0.1**	0.684	0.468	0.686	0.470	0.884	0.670	0.456
		Group 2	**0.1**	**0**	0.582	0.383	0.581	0.385	0.836	0.579	0.367
		Double	**0.1**	**0.1**	0.582	0.383	0.580	0.380	0.800	0.572	0.371
Main Effect Local Test	**15**	**Equal**	**0.1**	**0**	0.412	0.413	0.413	0.379	0.270	0.427	0.458
			0.1	**0.1**	0.424	0.406	0.417	0.372	0.233	0.446	0.410
		Group 2	**0.1**	**0**	0.294	0.293	0.296	0.267	0.206	0.292	0.307
		Double	**0.1**	**0.1**	0.326	0.304	0.291	0.253	0.160	0.330	0.324
	30	**Equal**	**0.1**	**0**	0.807	0.822	0.810	0.815	0.778	0.811	0.813
			0.1	**0.1**	0.817	0.800	0.818	0.790	0.759	0.816	0.786
		Group 2	**0.1**	**0**	0.689	0.696	0.693	0.701	0.670	0.687	0.697
		Double	**0.1**	**0.1**	0.707	0.691	0.708	0.693	0.638	0.704	0.694
Interaction Global Test	**15**	**Equal**	**0**	**0.1**	0.757	0.525	0.765	0.492	0.742	0.771	0.550
			0.1	**0.1**	0.767	0.537	0.753	0.494	0.728	0.783	0.557
		Group 2	**0**	**0.1**	0.706	0.502	0.694	0.444	0.726	0.719	0.515
		Double	**0.1**	**0.1**	0.674	0.460	0.679	0.422	0.668	0.667	0.483
	30	**Equal**	**0**	**0.1**	0.983	0.881	0.983	0.877	0.942	0.986	0.888
			0.1	**0.1**	0.977	0.899	0.980	0.894	0.936	0.977	0.906
		Group 2	**0**	**0.1**	0.959	0.842	0.958	0.831	0.922	0.954	0.838
		Double	**0.1**	**0.1**	0.950	0.839	0.952	0.821	0.890	0.945	0.828
Interaction Local Test	**15**	**Equal**	**0**	**0.1**	0.866	0.885	0.868	0.853	0.728	0.868	0.875
			0.1	**0.1**	0.876	0.861	0.872	0.850	0.740	0.876	0.883
		Group 2	**0**	**0.1**	0.843	0.831	0.834	0.800	0.664	0.850	0.843
		Double	**0.1**	**0.1**	0.808	0.793	0.811	0.761	0.612	0.818	0.805
	30	**Equal**	**0**	**0.1**	0.997	0.997	0.997	0.996	0.982	0.998	0.994
			0.1	**0.1**	0.992	0.993	0.993	0.991	0.983	0.994	0.991
		Group 2	**0**	**0.1**	0.991	0.987	0.991	0.985	0.954	0.990	0.986
		Double	**0.1**	**0.1**	0.989	0.984	0.988	0.982	0.947	0.989	0.986

Table 3: Hypothesis tests on the ADNI data. Global tests and all local tests with unadjusted p-values of < 0.05 are shown for Model 1.

	β_{CN}	β_{AD}	Test Statistic	Unadjusted p-value	Adjusted p-value
Model 1: One-step, Compound Symmetry Ψ_0 and Ψ_1, and Unstructured Σ					
Main Effects			42.86	0.154	
HCl and PCCl	0.037	0.189	3.39	0.024	0.315
HCl and PCCr	0.043	0.232	5.26	0.004	0.108
HCr and PCCr	0.011	0.168	3.63	0.018	0.315
PHCl and PQl	0.089	-0.093	4.83	0.030	0.315
PHCr and PQl	0.041	-0.136	4.59	0.031	0.315
Interactions			41.85	0.197	
HCl and PCCl	0.004	-0.011	5.85	0.002	0.090
HCl and PCCr	0.003	-0.014	7.82	0.001	0.045
HCr and PCCr	0.005	-0.009	4.49	0.009	0.209
PHCl and PCCr	0.008	-0.002	2.67	0.032	0.315

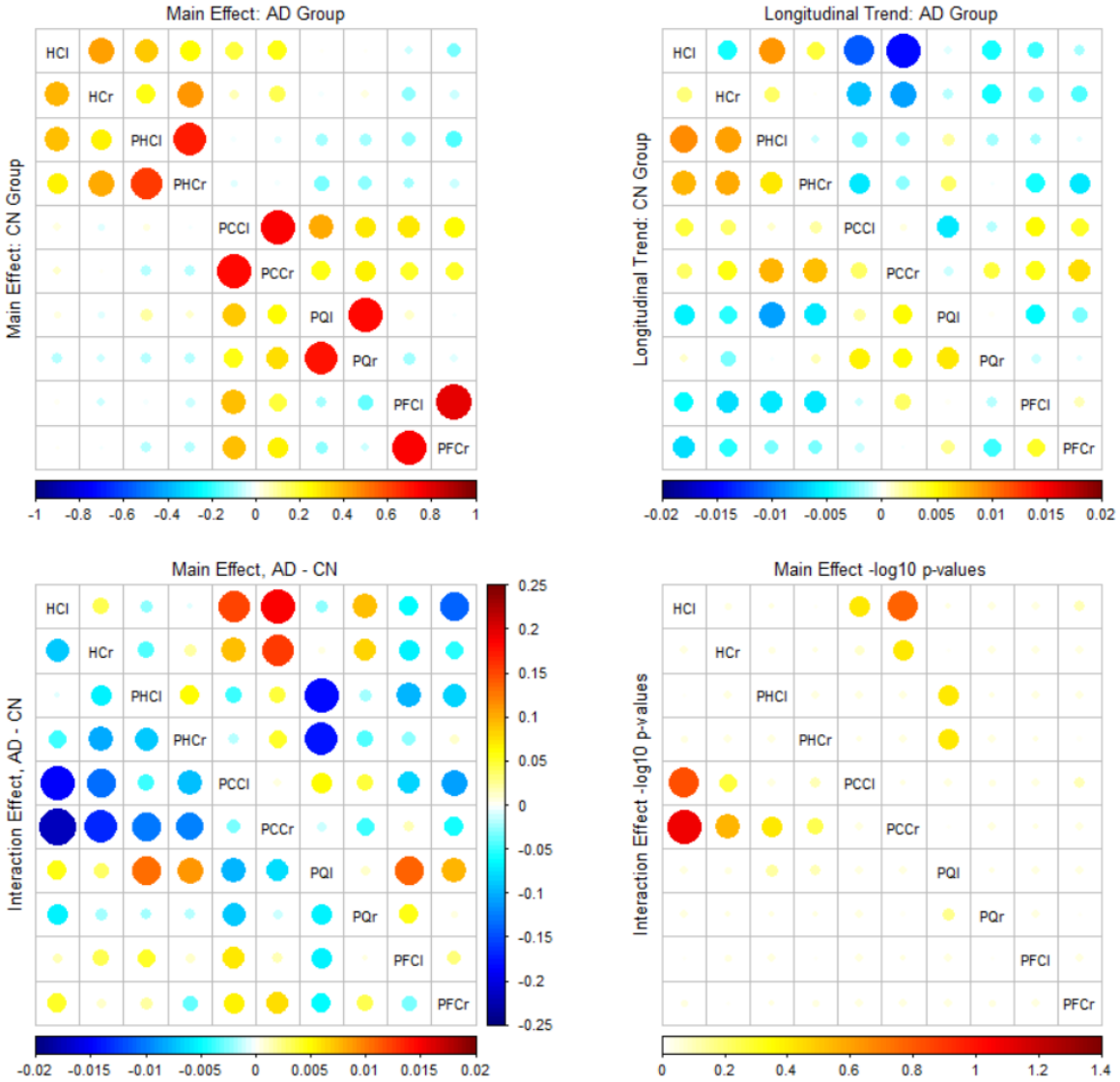

Figure 3: Model 1 results. Top left: A plot of the estimated intercept terms for the CN group (bottom left triangle) and AD group (top right triangle). Top right: A plot of the estimated slope terms for the CN group (bottom left triangle) and AD group (top right triangle). Bottom left: a plot of the group differences (AD estimates - CN estimates) for the estimated intercepts (top right triangle) and slopes (bottom left triangle). Bottom right: A plot of the $-\log_{10}$ corrected and adjusted p-values from all local hypothesis tests of group differences (AD estimates - CN estimates) for the estimated intercepts (top right triangle) and slopes (bottom left triangle).

inflation is somewhat attenuated by the increase in sample size from 15 to 30 per group. Table 2 demonstrates adequate power, both locally and globally for all three models. As expected, power increased with larger group size and decreased with a larger true group 2 variance.

There was no consistent difference in performance between the three models in terms of power or Type I error across the different simulation settings. The two full variance settings match the true model of the simulated data, yet the reduced variance model does not seem to suffer in comparison. While the reduced variance model is not the true model, it may offer similar performance because of the reduction in the parameter space allowing for improved estimation. The reduced variance model does not capture the full true variance, but it still performs well by allowing the connectivity for each ROI pair to be correlated across multiple visits for a given subject.

Overall, the full convergence results do not consistently improve on the one-step estimator results. With little to nothing to gain in terms of power and Type I error, the additional computational resources used by the full-convergence model do not seem to offer any practical advantage. One of the main differences in the performance of the three models is the computational time. Table 4 shows the relative timing of the three models fit to each simulation scenario. The full convergence model takes, on average, over 2.5 times longer to run without seeing any notable boost in performance. For reference, using a 3.7 GHz Quad-Core Intel Xeon with 16GB ram, the average times for fitting the one-step full variance model with 30 subjects per group for 3, 5, and 10 ROIs were 3.8 seconds, 54.9 seconds, and 87.2 minutes, respectively. These results show that the time increases quickly with the dimension of the model. The computational time is largely driven by the permutation procedure. Thus, if a larger number of permutations is desired for the testing procedure, then the computational time will also increase.

Table 4: Average relative timing of the three models considered in the simulation study.

Convergence Type	Variance Structure	Relative Time
Full	Full	2.56
One-Step	Full	1.02
One-Step	Reduced	1.00

4.2 ADNI Data

The four models fit to the ADNI data present slightly different results. The difference between Model 1 and Model 2 is very minimal. The nearly identical results provide further support of the conclusion from the simulation study that the full convergence and one-step estimator models lead to very similar estimates and inference. Some more pronounced differences in results arise when Model 1 is compared with Models 3 and 4. These differences make sense considering that Model 4 does not account for the within-subject dependence of the FC and thus appears to suffer from diminished power to detect group differences.

The more interesting differences exist in comparing Models 1 and 3, but some common patterns run throughout both sets of results. In both models, many of the local hypotheses that were significant prior to the FDR correction appear between the HC/PHC and the PCC. These groups differences strengthen the one local hypothesis that is significant after FDR correction from Models 1 and 2 which shows a significantly larger decrease in connectivity between the HCl and PCCr in the AD group than in the CN group. While the significant results disappears after FDR correction, the fact that many other HC/PHC connections with the PCC see a similar pattern helps to indicate differing baseline and longitudinal trend effects in the FC of the two groups. This clustering of group differences can be seen in Figure 3 with the smallest p-values (red and orange circles) appearing between the HC/PHC and PCC. Furthermore, this apparent difference in FC between the HC and PCC supports previous reports in the literature. Wang et al. [2006], Sorg et al. [2007], and Greicius et al. [2004] all noted decreased FC between the HC and PCC in patients with AD in analyses of cross-sectional data. Similar results from Supekar et al. [2008] showed decreased clustering coefficients for the HC. Our analysis confirms these results with the addition of a longitudinal component to the analysis. Our results not only conclude that AD and CN patients have differing FC between the HC and PCC, as the previous works have shown, but we also more clearly describe the differences in baseline and trend in connectivity between these two regions.

4.3 Current Limitations and Future Work

Our familiar linear model framework utilized in this paper allows for easy adoption and understanding of the model and its results. Additionally, the linear model framework offers many natural extensions, including terms for additional covariates such as scanner effect or gender and different structures for the variance components to capture a wider range of possible correlation structures.

Our current method has the advantage of allowing for joint modeling of a complete FC network rather than taking a massive univariate approach. We see this joint modeling as a significant step forward, but complete brain analyses are still not yet feasible due to high computational demands of a model fit to many ROIs and the limited sample size of many fMRI studies. Here we have fit models to 10 ROI networks, but many brain atlases include at least 100 regions. In the future, some form of regularization could be introduced into the model to allow for analysis of an entire brain atlas.

The selection of the proper structure for the variance components deserves more attention. While a block compound symmetry structure for Ψ has a natural interpretation similar to that of a random intercept, it is certainly possible to conceive of other viable structures. Choosing between structures is not a trivial task. One way to alleviate the model selection dilemma is to introduce a more robust sandwich type estimator of $\widehat{\text{Var}}(\hat{\beta})$, in which case incorrect specification of the variance would only lead to reduced power.

5 Conclusions

We have introduced a novel variance components longitudinal model to estimate and draw inference on the group differences in FC using resting-state fMRI data. The model properly accounts for the correlation inherent in repeated measures data and the autocorrelation present in fMRI time series. A permutation testing procedure performs global and local two-sample testing in an efficient manner. The linear model framework and utilization of generalized least squares estimators offers great simplicity and a large number of natural extensions.

As a practical example, we applied the method to resting-state fMRI data from the ADNI database. Our analysis found a faster decline in FC between the left hippocampus and the right posterior cingulate cortex in AD patients compared to the CN control group. This finding confirms the results of previous studies and helps solidify the central roles of the hippocampus and default mode network in AD.

6 Acknowledgments

Data collection and sharing for this project was funded by the ADNI (National Institutes of Health Grant U01 AG024904) and DOD ADNI (Department of Defense award number W81XWH-12-2-0012). ADNI is funded by the National Institute on Aging, the National Institute of Biomedical Imaging and Bioengineering, and through generous contributions from the following: AbbVie, Alzheimers Association; Alzheimers Drug Discovery Foundation; Araclon Biotech; BioClinica, Inc.; Biogen; Bristol-Myers Squibb Company; CereSpir, Inc.; Cogstate; Eisai Inc.; Elan Pharmaceuticals, Inc.; Eli Lilly and Company; EuroImmun; F. Hoffmann-La Roche Ltd and its affiliated company Genentech, Inc.; Fujirebio; GE Healthcare; IXICO Ltd.; Janssen Alzheimer Immunotherapy Research & Development, LLC.; Johnson & Johnson Pharmaceutical Research & Development LLC.; Lumosity; Lundbeck; Merck & Co., Inc.; Meso Scale Diagnostics, LLC.; NeuroRx Research; Neurotrack Technologies; Novartis Pharmaceuticals Corporation; Pfizer Inc.; Piramal Imaging; Servier; Takeda Pharmaceutical Company; and Transition Therapeutics. The Canadian Institutes of Health Research is providing funds to support ADNI clinical sites in Canada. Private sector contributions are facilitated by the Foundation for the National Institutes of Health (`www.fnih.org`). The grantee organization is the Northern California Institute for Research and Education, and the study is coordinated by the Alzheimers Therapeutic Research Institute at the University of Southern California. ADNI data are disseminated by the Laboratory for Neuro Imaging at the University of Southern California.

7 Supplement

Supplement A: Supplemental Tables and Figures Table S1 of this supplement shows additional simulation study Type I error results. Table S2 shows significant results from Models 2, 3, and 4 in table form. Figures S1, S2, and S3 present the modeling results graphically.

References

Takeshi Amemiya. A note on a heteroscedastic model. *Journal of Econometrics*, 6(3):365–370, 1977.

Yoav Benjamini and Yosef Hochberg. Controlling the false discovery rate: a practical and powerful approach to multiple testing. *Journal of the Royal Statistical Society. Series B (Methodological)*, pages 289–300, 1995.

Alex Chase. Altered functional connectivity in preclinical dementia. *Nature Reviews Neurology*, 10(11), 2014.

Pin-Yu Chen, Jeng-Min Chiou, Ya-Fang Yang, Yu-Ting Chen, Hsin-Long Hsieh, Yu-Ling Chang, and Wen-Yih I Tseng. Heterogeneous aging effects on functional connectivity in different cortical regions: A resting-state functional mri study using functional data analysis. *PLOS ONE*, 11(9):e0162028, 2016.

EunYi Chung, Joseph P Romano, et al. Exact and asymptotically robust permutation tests. *The Annals of Statistics*, 41(2):484–507, 2013.

Mark Fiecas, Ivor Cribben, Reyhaneh Bahktiari, and Jacqueline Cummine. A variance components model for statistical inference on functional connectivity networks. *NeuroImage*, 149:256–266, 2017.

Emily S Finn and R Todd Constable. Individual variation in functional brain connectivity: implications for personalized approaches to psychiatric disease. *Dialogues in Clinical Neuroscience*, 18(3):277, 2016.

Michael D Fox and Marcus E Raichle. Spontaneous fluctuations in brain activity observed with functional magnetic resonance imaging. *Nature Reviews Neuroscience*, 8(9):700, 2007.

Habib Ganjgahi, Anderson M Winkler, David C Glahn, John Blangero, Peter Kochunov, and Thomas E Nichols. Fast and powerful heritability inference for family-based neuroimaging studies. *NeuroImage*, 115:256–268, 2015.

Michael D Greicius, Gaurav Srivastava, Allan L Reiss, and Vinod Menon. Default-mode network activity distinguishes alzheimer's disease from healthy aging: evidence from functional mri. *Proceedings of the National Academy of Sciences of the United States of America*, 101(13):4637–4642, 2004.

Anne Hafkemeijer, Jeroen van der Grond, and Serge ARB Rombouts. Imaging the default mode network in aging and dementia. *Biochimica et Biophysica Acta (BBA)-Molecular Basis of Disease*, 1822(3):431–441, 2012.

Dominic Holland, Rahul S Desikan, Anders M Dale, Linda K McEvoy, Alzheimers Disease Neuroimaging Initiative, et al. Rates of decline in alzheimer disease decrease with age. *PLOS ONE*, 7(8):e42325, 2012.

Nan Laird. Analysis of longitudinal and cluster-correlated data. In *NSF-CBMS Regional Conference Series in Probability and Statistics*, pages i–155. JSTOR, 2004.

Yuxia Li, Xiaoni Wang, Yongqiu Li, Yu Sun, Can Sheng, Hongyan Li, Xuanyu Li, Yang Yu, Guanqun Chen, Xiaochen Hu, et al. Abnormal resting-state functional connectivity strength in mild cognitive impairment and its conversion to alzheimers disease. *Neural Plasticity*, 2016, 2015.

Guy Melard, Marianne Paesmans, and Roch Roy. Consistent estimation of the asymptotic covariance structure of multivariate serial correlations. *Journal of Time Series Analysis*, 12(4):351–361, 1991.

Marek Omelka and Markus Pauly. Testing equality of correlation coefficients in two populations via permutation methods. *Journal of Statistical Planning and Inference*, 142(6):1396–1406, 2012.

Belinda Phipson, Gordon K Smyth, et al. Permutation p-values should never be zero: calculating exact p-values when permutations are randomly drawn. *Stat Appl Genet Mol Biol*, 9(1):Article39–Article39, 2010.

Ping Ren, Raymond Y Lo, Benjamin P Chapman, Mark Mapstone, Anton Porsteinsson, and Feng Lin. Longitudinal alteration of intrinsic brain activity in the striatum in mild cognitive impairment. *Journal of Alzheimer's Disease*, 54(1):69–78, 2016.

Roch Roy. Asymptotic covariance structure of serial correlations in multivariate time series. *Biometrika*, pages 824–827, 1989.

Christian Sorg, Valentin Riedl, Mark Mühlau, Vince D Calhoun, Tom Eichele, Leonhard Läer, Alexander Drzezga, Hans Förstl, Alexander Kurz, Claus Zimmer, et al. Selective changes of resting-state networks in individuals at risk for alzheimer's disease. *Proceedings of the National Academy of Sciences*, 104(47):18760–18765, 2007.

Kaustubh Supekar, Vinod Menon, Daniel Rubin, Mark Musen, and Michael D Greicius. Network analysis of intrinsic functional brain connectivity in alzheimer's disease. *PLoS Comput Biol*, 4(6):e1000100, 2008.

Cajo JF Ter Braak. Permutation versus bootstrap significance tests in multiple regression and anova. In *Bootstrapping and related techniques*, pages 79–85. Springer, 1992.

Wiesje M van der Flier, Yolande AL Pijnenburg, Nick C Fox, and Philip Scheltens. Early-onset versus late-onset alzheimer's disease: the case of the missing apoe 4 allele. *The Lancet Neurology*, 10(3):280–288, 2011.

Kun Wang, Meng Liang, Liang Wang, Lixia Tian, Xinqing Zhang, Kuncheng Li, and Tianzi Jiang. Altered functional connectivity in early alzheimer's disease: a resting-state fmri study. *Human Brain Mapping*, 28(10): 967–978, 2007.

Liang Wang, Yufeng Zang, Yong He, Meng Liang, Xinqing Zhang, Lixia Tian, Tao Wu, Tianzi Jiang, and Kuncheng Li. Changes in hippocampal connectivity in the early stages of alzheimer's disease: evidence from resting state fmri. *NeuroImage*, 31(2):496–504, 2006.

Liang Wang, Catherine M Roe, Abraham Z Snyder, Matthew R Brier, Jewell B Thomas, Chengjie Xiong, Tammie L Benzinger, John C Morris, and Beau M Ances. Alzheimer disease family history impacts resting state functional connectivity. *Annals of Neurology*, 72(4):571–577, 2012.

Anderson M Winkler, Gerard R Ridgway, Matthew A Webster, Stephen M Smith, and Thomas E Nichols. Permutation inference for the general linear model. *NeuroImage*, 92:381–397, 2014.

Keith J Worsley and Karl J Friston. Analysis of fmri time-series revisitedagain. *NeuroImage*, 2(3):173–181, 1995.

Jie Xiang, Hao Guo, Rui Cao, Hong Liang, Junjie Chen, et al. An abnormal resting-state functional brain network indicates progression towards alzheimer's disease. *Neural Regeneration Research*, 8(30):2789, 2013.

Supplement A: Supplemental Tables and Figures

Table S1: Type I error rates for simulation study. Type I errors for the main effect (group difference in intercepts) and interaction effect (group difference in slopes) are reported both globally and locally. The global Type I errors are averaged across all models. The local Type I errors reported are unadjusted and averaged across all simulations and all null ROI pairs.

		Convergence Type:			**Full**		**One-Step**			**One-Step**	
		Variance Structure:			**Full**		**Full**			**Reduced**	
	Group Size	**Variance**	β_0	β_1	**3 ROIs**	**5 ROIs**	**3 ROIs**	**5 ROIs**	**10 ROIs**	**3 ROIs**	**5 ROIs**
Main Effect Local Test	**15**	**Equal**	**0.1**	**0.1**	0.050	0.062	0.050	0.067	0.069	0.054	0.066
			0.1	**0**	0.054	0.060	0.050	0.057	0.067	0.056	0.061
		Group 2	**0.1**	**0.1**	0.061	0.064	0.056	0.062	0.067	0.057	0.062
		Double	**0.1**	**0**	0.066	0.065	0.068	0.061	0.064	0.066	0.063
	30	**Equal**	**0.1**	**0.1**	0.052	0.057	0.053	0.057	0.054	0.053	0.059
			0.1	**0**	0.048	0.058	0.046	0.057	0.054	0.048	0.057
		Group 2	**0.1**	**0.1**	0.054	0.059	0.057	0.057	0.056	0.052	0.057
		Double	**0.1**	**0**	0.056	0.059	0.057	0.057	0.056	0.060	0.057
Interaction Local Test	**15**	**Equal**	**0.1**	**0.1**	0.060	0.062	0.060	0.068	0.073	0.060	0.063
			0	**0.1**	0.072	0.062	0.074	0.068	0.073	0.072	0.060
		Group 2	**0.1**	**0.1**	0.058	0.067	0.055	0.065	0.069	0.061	0.065
		Double	**0**	**0.1**	0.068	0.060	0.070	0.061	0.073	0.066	0.062
	30	**Equal**	**0.1**	**0.1**	0.056	0.054	0.054	0.056	0.054	0.056	0.057
			0	**0.1**	0.058	0.058	0.054	0.057	0.057	0.054	0.058
		Group 2	**0.1**	**0.1**	0.062	0.053	0.064	0.055	0.056	0.063	0.053
		Double	**0**	**0.1**	0.064	0.054	0.062	0.053	0.060	0.062	0.053

Table S2: Hypothesis tests on the ADNI data. Global tests and all local tests with unadjusted p-values of < 0.05 are shown for Models 2-4.

	β_{CN}	β_{AD}	Test Statistic	Unadjusted p-value	Adjusted p-value
Model 2: Full Convergence, Compound Symmetry Ψ_0 and Ψ_1, and Unstructured Σ					
Main Effects			42.06	0.156	
HCl and PCCl	0.037	0.189	3.35	0.024	0.317
HCl and PCCr	0.043	0.232	5.14	0.004	0.111
HCr and PCCr	0.010	0.168	3.57	0.019	0.317
PHCl and PQl	0.089	-0.093	4.79	0.030	0.317
PHCr and PQl	0.042	-0.136	4.56	0.029	0.317
Interactions			41.26	0.199	
HCl and PCCl	0.004	-0.011	5.77	0.002	0.081
HCl and PCCr	0.003	-0.014	7.65	¡0.001	0.027
HCr and PCCr	0.005	-0.009	4.41	0.010	0.218
PHCl and PCCr	0.008	-0.002	2.61	0.032	0.317
Model 3: One-step, Scaled Identity Ψ_0 and Ψ_1, and Diagonal Σ					
Main Effects			47.75	0.312	
HCl and PCCl	0.058	0.228	3.95	0.021	0.367
HCl and PCCr	0.068	0.269	5.51	0.005	0.150
PHCl and PQl	0.125	-0.074	5.37	0.033	0.367
PHCr and PQl	0.056	-0.164	6.57	0.009	0.207
PCCl and PFCr	0.381	0.240	2.86	0.033	0.367
Interactions			54.90	0.238	
HCl and PCCl	0.002	-0.013	5.14	0.005	0.150
HCl and PCCr	0.000	-0.017	6.49	0.017	0.150
PHCl and PCCr	0.007	-0.003	2.75	0.037	0.367
PHCl and PQl	-0.011	0.003	4.71	0.049	0.403
PHCr and PQl	-0.007	0.006	3.66	0.047	0.403
PQl and PQr	0.007	0.000	1.31	0.035	0.367
Model 4: One-step, Scaled Identity Ψ_0, Zero Ψ_1, and Diagonal Σ					
Main Effects			62.65	0.412	
HCl and PCCr	0.078	0.281	8.41	0.013	0.513
PHCr and PQl	0.040	-0.162	6.61	0.023	0.513
PCCl and PFCr	0.402	0.223	4.35	0.018	0.513
Interactions			68.63	0.317	
HCl and PCCl	0.000	-0.013	5.60	0.036	0.592
HCl and PCCr	-0.001	-0.018	9.11	0.006	0.513
PHCl and PCCr	0.006	-0.004	3.83	0.040	0.592

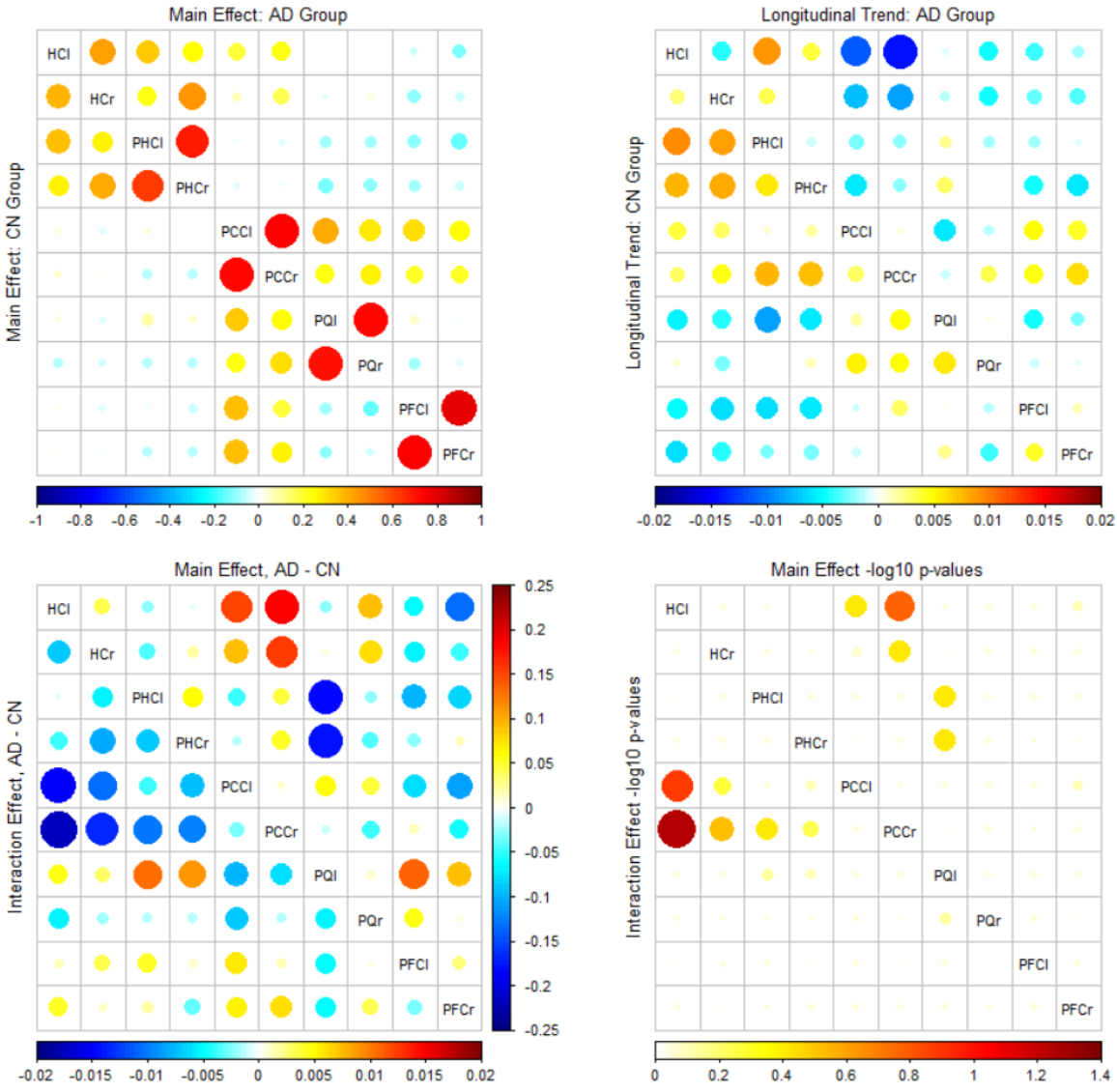

Figure S1: Model 2 results. Top left: A plot of the estimated intercept terms for the CN group (bottom left triangle) and AD group (top right triangle). Top right: A plot of the estimated slope terms for the CN group (bottom left triangle) and AD group (top right triangle). Bottom left: a plot of the group differences (AD estimates - CN estimates) for the estimated intercepts (top right triangle) and slopes (bottom left triangle). Bottom right: A plot of the $-\log_{10}$ corrected and adjusted p-values from all local hypothesis tests of group differences (AD estimates - CN estimates) for the estimated intercepts (top right triangle) and slopes (bottom left triangle).

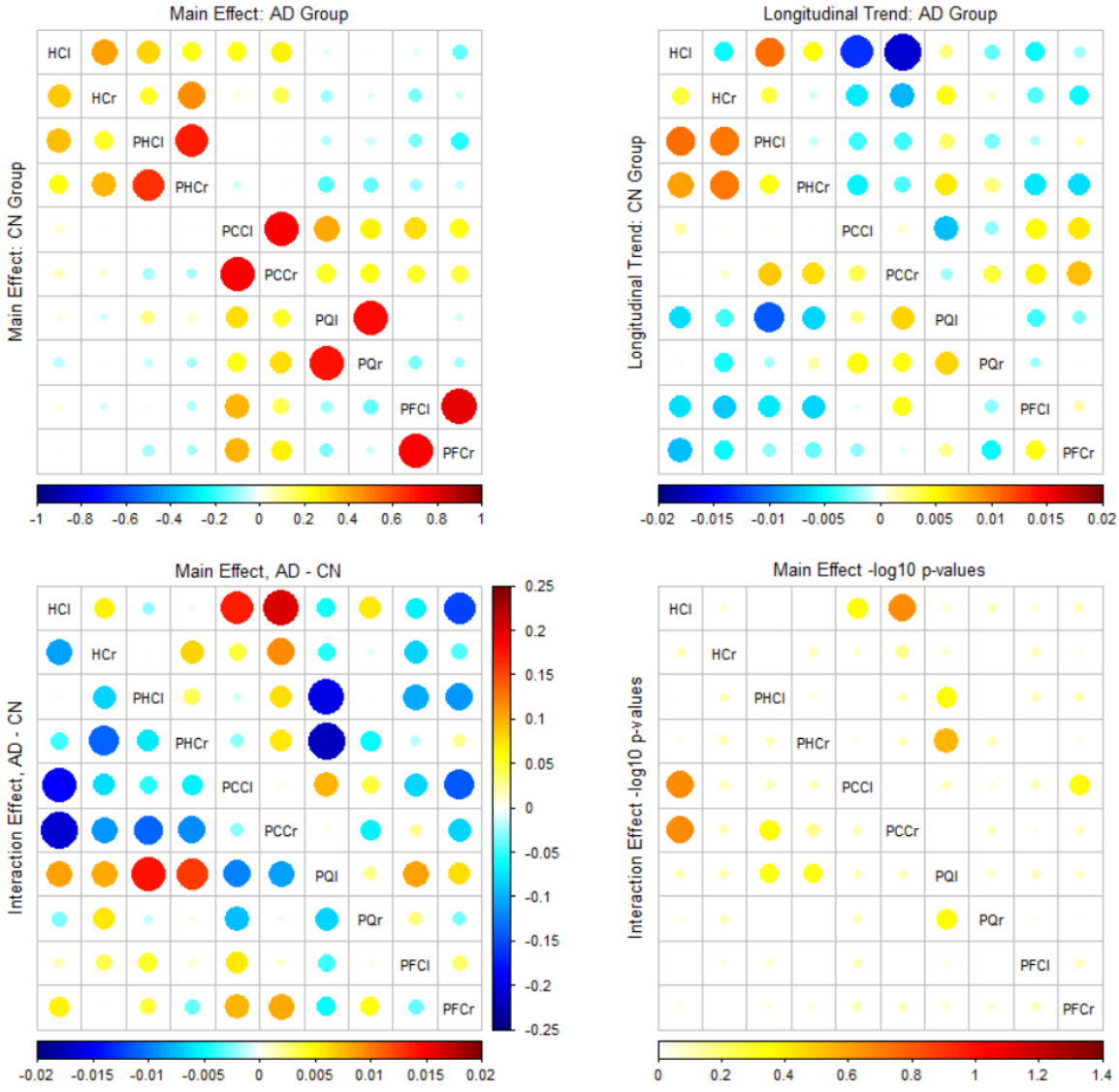

Figure S2: Model 3 results. Top left: A plot of the estimated intercept terms for the CN group (bottom left triangle) and AD group (top right triangle). Top right: A plot of the estimated slope terms for the CN group (bottom left triangle) and AD group (top right triangle). Bottom left: a plot of the group differences (AD estimates - CN estimates) for the estimated intercepts (top right triangle) and slopes (bottom left triangle). Bottom right: A plot of the $-\log_{10}$ corrected and adjusted p-values from all local hypothesis tests of group differences (AD estimates - CN estimates) for the estimated intercepts (top right triangle) and slopes (bottom left triangle).

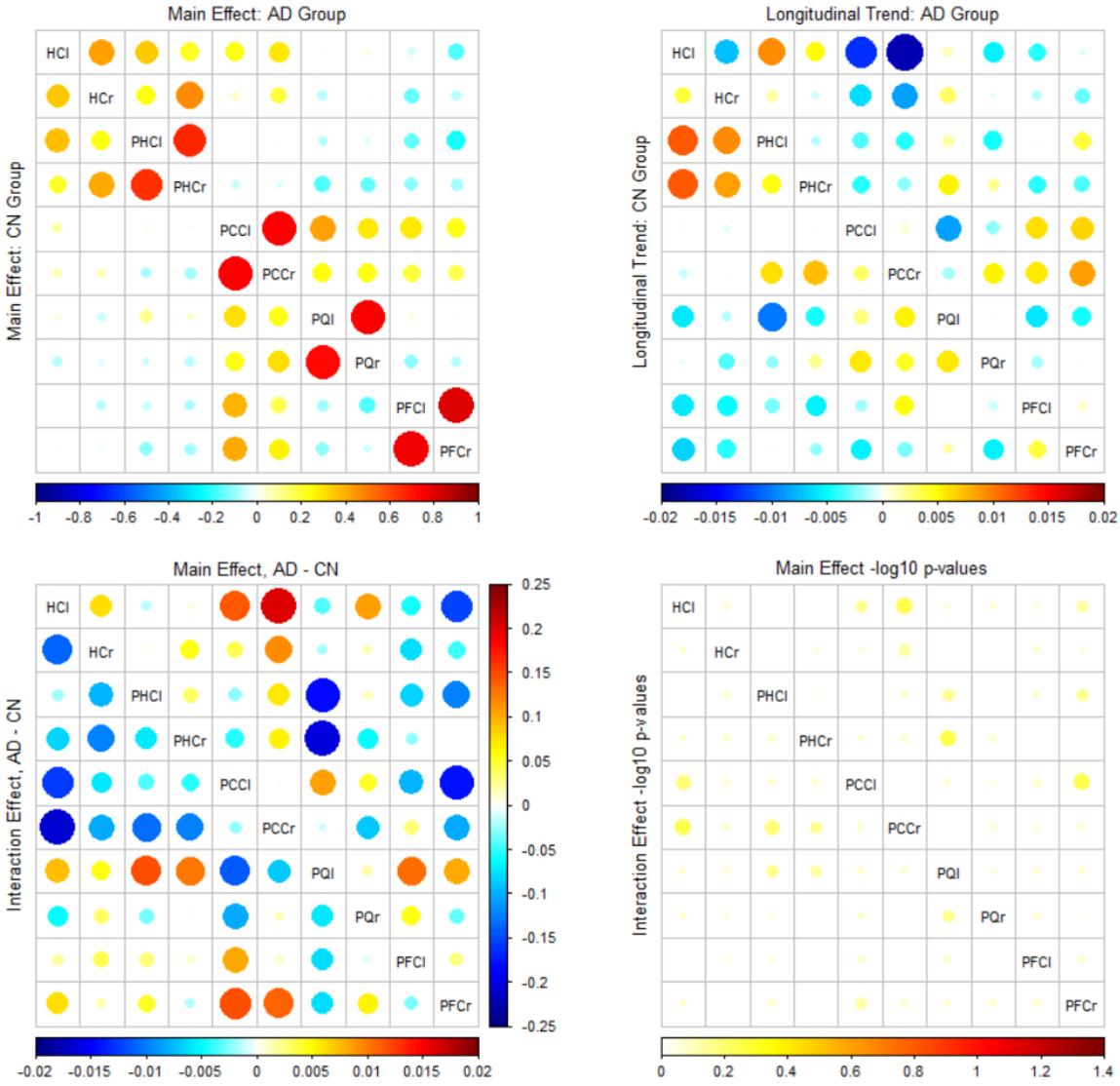

Figure S3: Model 4 results. Top left: A plot of the estimated intercept terms for the CN group (bottom left triangle) and AD group (top right triangle). Top right: A plot of the estimated slope terms for the CN group (bottom left triangle) and AD group (top right triangle). Bottom left: a plot of the group differences (AD estimates - CN estimates) for the estimated intercepts (top right triangle) and slopes (bottom left triangle). Bottom right: A plot of the $-\log_{10}$ corrected and adjusted p-values from all local hypothesis tests of group differences (AD estimates - CN estimates) for the estimated intercepts (top right triangle) and slopes (bottom left triangle).